Atmospheric
Chemistry
and Physics
Discussions

1 **Estimating CCN number concentrations using aerosol optical properties:**

2 **Role of particle number size distribution and parameterization**

3

4 Yicheng Shen[1,2], Aki Virkkula [2,1,3], Aijun Ding[1], Krista Luoma[2], Helmi Keskinen [2,4], Pasi P. Aalto [2],

5 Xuguang Chi[1], Ximeng Qi[1], Wei Nie[1], Xin Huang[1],

6 Tuukka Petäjä[2,1], Markku Kulmala[2], Veli-Matti Kerminen[2]

7

8 [1]Joint International Research Laboratory of Atmospheric Sciences, School of Atmospheric Sciences,

9 Nanjing University, Nanjing, 210023, China

10 [2]Institute for Atmospheric and Earth System Research, University of Helsinki, Helsinki, Finland

11 [3]Finnish Meteorological Institute, Helsinki, Finland

12 [4]Hyytiälä Forestry Field Station, Hyytiäläntie 124, Korkeakoski FI 35500, Finland

13

14 Keywords: CCN, scattering coefficient, backscatter fraction, Ångström exponent

15

16 **Abstract**

17 The concentration of cloud condensation nuclei (CCN) is an essential parameter affecting

18 aerosol-cloud interactions within warm clouds. Long-term CCN number concentration (N_{CCN})

19 data are scarce, there are a lot more data on aerosol optical properties (AOPs). It is therefore

20 valuable to derive parameterizations for estimating N_{CCN} from AOP measurements. Such

21 parameterizations have been made earlier, in the present work a new one is presented. The

22 relationships between AOPs, N_{CCN} and particle number size distributions were investigated

23 based on in-situ measurement data from six stations in very different environments around the

24 world. The parameterization derived here depends on the scattering Ångström exponent (SAE),

25 backscatter fraction (BSF) and total scattering coefficient (σ_{sp}) of PM10 particles. The analysis

26 showed that the dependence of N_{CCN} on supersaturation SS% is logarithmic:

27 $N_{CCN} \approx ((287 \pm 45)SAE_{10}\ln(SS\%/(0.093 \pm 0.006))(BSF - BSF_{min}) + (5.2 \pm 3.3))\sigma_{sp}$.

28 At the lowest supersaturations of each site (SS% ≈ 0.1) the average bias, defined as the ratio of the

29 AOP-derived and measured N_{CCN} varied from ~0.7 to ~1.5 at most sites except at a Himalayan site

30 where bias was > 4. At SS% > 0.3 the average bias ranged from ~0.7 to ~1.3 at all sites. In other

Atmospheric
Chemistry
and Physics
Discussions

1   words, at SS% > 0.3 N_{CCN} was estimated with an average uncertainty of approximately 30% by

2   using nephelometer data. The squared correlation coefficients between the AOP-derived and

3   measured N_{CCN} varied from ~0.5 to ~0.8. The coefficients of the parameterization derived for the

4   different sites were linearly related to each other. To study the explanation of this, lognormal

5   unimodal particle size distributions were generated and N_{CCN} and AOPs were calculated. The

6   simulation yielded similar relationships between the coefficients as in the field data. It also

7   showed that the relationships of the coefficients are affected by the geometric mean diameter

8   and width of the size distribution and the activation diameter.

9

10   **1. Introduction**

11   Aerosol-cloud interactions (ACI) are the most significant sources of uncertainty in estimating

12   the radiative forcing of the Earth's climate system (e.g., Forster et al., 2007; Kerminen et al.,

13   2012), which makes it more challenging to predict the future climate change (Schwartz et al.,

14   2010). An essential parameter affecting ACI within warm clouds is cloud condensation nuclei

15   (CCN) concentration, the number concentration of particles capable of initiating cloud droplet

16   formation at a given supersaturation. Determining CCN concentrations and their temporal and

17   spatial variations is one of the critical aspects to reduce such uncertainty.

18

19   CCN number concentrations (N_{CCN}) have been measured at different locations worldwide (e.g.,

20   Twomey, 1959; Hudson,1993; Kulmala et al., 1993; Hämeri et al., 2001; Sihto et al., 2011;

21   Pöhlker et al., 2016; Ma et al., 2014). However, the accessible data especially for long-term

22   measurement is still limited in the past and nowadays due to the relatively higher cost of

23   instrumentation and the complexity of long-term operating. As an alternative to direct

24   measurement, N_{CCN} can also be estimated from particle number size distributions and chemical

25   composition using the Köhler equation. Several studies have investigated the relative

26   importance of the chemical composition and particle number distributions (Dusek et al., 2006;

27   Ervens et al., 2007; Hudson, 2007; Crosbie et al., 2015). For the best of our understanding, the

28   particle number size distributions are more important in determining N_{CCN} than aerosol

29   chemical composition. This makes particle number size distribution measurements capable of

Atmospheric
Chemistry
and Physics
Discussions

1   serving as a supplementary of direct CCN measurements.

2

3   Considering the tremendous spatiotemporal heterogeneity of atmospheric aerosol, neither

4   direct measurements of N_{CCN} of the concentrations estimated from particle size distribution are

5   adequate for climate research. In order to overcome the limitation of current measurements,

6   many studies have attempted to estimate N_{CCN} using aerosol optical properties (AOPs) (e.g.,

7   Ghan et al., 2006; Shinozuka et al., 2009; Andreae, 2009; Jefferson, 2010; Liu et al., 2014;

8   Shinozuka et al., 2015; Tao et al., 2018). Most of these studies attempted to link N_{CCN} with

9   extensive AOPs, such as the aerosol extinction coefficient (σ_{ext}), aerosol scattering coefficient

10   (σ_{sp}) and aerosol optical depth (AOD). Both N_{CCN} and σ_{sp} are extensive properties that vary

11   with a varying aerosol loading. The most straightforward approach to estimate CCN is to utilize

12   the ratio between CCN and one of the extensive AOPs (e.g. AOD, σ_{ext}, σ_{sp}). However, the ratio

13   is not a constant. Previous studies have also pointed out that the relationship between N_{CCN} and

14   extensive AOPs are nonlinear. On one hand, Andreae (2009) reported that the relationship

15   between AOD and CCN number concentration at the supersaturation of 0.4% ($CCN_{0.4}$) can be

16   written as $AOD_{500}=0.0027 \cdot (CCN_{0.4})^{0.640}$, which indicates AOT and CCN depend in a non-linear

17   way on each other: for a larger AOD there are more CCN per-unit change in AOD. On the other

18   hand, Shinozuka et al. (2015) indicated that the larger the extinction coefficient σ_{ext} was, the

19   fewer CCN were per unit change of σ_{ext}.

20

21   Some studies have also involved intensive aerosol optical properties, such as the scattering

22   Ångström exponent (SAE), hemispheric backscattering fraction (BSF) and single-scattering

23   albedo (SSA) to build up a bridge between the N_{CCN} and AOPs. Jefferson (2010) used BSF and

24   SSA to parameterize the coefficients C and k to present $N_{CCN}(SS\%) = C \times (SS\%)^k$, where SS%

25   is the supersaturation percent (Twomey, 1959). Liu and Li (2014) discussed how different

26   aerosol properties affect the ratio of N_{CCN} to σ_{sp}, i.e., R_{CCN}/σ_{sp} based on *in-situ* and remote-

27   sensing data. Shinozuka et al. (2015) used SAE and aerosol extinction coefficient to estimate

28   N_{CCN}. Tao et al. (2018) used a novel method to derive the ratio R_{CCN}/σ_{sp} which they named as

29   AR_{sp}, based on SAE and aerosol hygroscopicity using a humidified nephelometer. All the

Atmospheric
Chemistry
and Physics
Discussions

1   studies mentioned above noted that the particle number size distribution (PNSD) plays an

2   important role in estimating N_{CCN} from aerosol optical properties.

3

4   In this study, we will introduce a new approach to estimate N_{CCN}, along with a brief discussion

5   on how the ratio between N_{CCN} and σ_{sp} is related to BSF. The AOPs needed in our estimation

6   are σ_{sp}, BSF and SAE obtained using a 3-wavelength nephelometer, either the TSI 3563 or

7   Ecotech Aurora 3000. The main goal of this study is to provide a parameterization for

8   calculating N_{CCN} using AOPs, and to probe the physical explanations behind this

9   parameterization. The method will be applied to six different sites worldwide.

10

11   **2. Methods**

12   **2.1 Sites and measurements**

13   In-situ measurements of AOPs, PNSDs, and N_{CCN} were conducted at SMEAR II in Finland,

14   SORPES in China, and 4 ARM Climate Research Facility (ACRF) sites (Mather and Voyles,

15   2013). The locations and measurement periods are listed in Table 1.

16

17   The Station for Measuring Forest Ecosystem-Atmosphere Relations (**SMEAR II**) is located at

18   the Hyytiälä Forestry Field Station (61°51' N, 24°17' E, 181 m above sea level) of University

19   of Helsinki, 60 km north-east from the nearest city. The station represents boreal coniferous

20   forest, which covers ~8 % of the Earth's surface. Total scattering coefficient (σ_{sp}) and

21   hemispheric backscattering coefficient (σ_{bsp}) of sub-1 μm and sub-10 μm particles are measured

22   using a TSI-3563 3-wavelength integrating nephelometer at λ = 450, 550, and 700 nm. The

23   calibration, data processing, and calculation of AOPs followed the procedure described by

24   Virkkula et al. (2011) and Luoma et al. (2018). N_{CCN} was measured at supersaturations (SS%)

25   of 0.1%, 0.2%, 0.3%, 0.5% and 1.0% using a DMT CCN-100 CCN counter, likewise in

26   Schmale et al. (2017). A whole measurement cycle takes around 2 hours; data were interpolated

27   to hourly time resolution to compare with other measurements. Particle number size

28   distributions (PNSD) were measured with a custom-made Differential Mobility Particle Sizer

29   (DMPS) system in size range 3−1000 nm (Aalto et al., 2001). A more detailed description of

1 CCN measurements and station operation can be found in Sihto et al. (2011) and Paramonov et

2 al. (2015).

3

4 The Station for Observing Regional Processes of the Earth System (**SORPES**) is located at a

5 suburb of Nanjing, a megacity in the Yangtze River Delta municipal aggregation (32°07'14" N,

6 118°57'10" E; ~40m a.s.l.). σ_{sp} and σ_{bsp} of total suspended particles (TSP) are measured with

7 an Ecotech Aurora-3000 3-wavelength integrating nephelometer at $\lambda = 450$, 525, and 635 nm

8 as described by Shen et al. (2018). N_{CCN} is measured using a CCN-200 dual column CCN

9 counter at 5 supersaturations: 0.1%, 0.2%, 0.4%, 0.6% and 0.8%. The two columns make the

10 same cycle simultaneously to cross-check with each other. Each cycle takes 30 minutes. PNSD

11 in the size range of 6 - 800 nm are measured with a DMPS built by University of Helsinki.

12 More details of the measurements at SORPES are given by, e.g., Ding et al. (2013, 2016) and

13 Qi et al. (2015).

14

15 The US Atmospheric Radiation Measurement (ARM) Mobile Facility (AMF) measures

16 atmospheric aerosol and radiation properties all over the world. The first AMF (AMF1) was

17 deployed in 2005 with both a CCN counter and a nephelometer. Between 2011 and 2018, AMF1

18 is operated at four locations: Ganges Valley (**PGH**) in the Himalayas, Cape Cod, Massachusetts

19 (**PVC**) in a coastal area of U.S., Manacapuru (**MAO**) inside the Amazonian rain forest, and

20 Ascension Island (**ASI**) on the South Atlantic Ocean downwind from Africa. Three of them are

21 accompanied by a scanning mobility particle sizer (SMPS; Kuang, 2016). The SMPS is also

22 part of the Aerosol Observing System (AOS) running side by side with AMF1 since 2012. Both

23 PNSD and AOPs are available simultaneously at PVC, MAO, and ASI. σ_{sp} and σ_{bsp} of sub-1

24 μm and sub-10 μm particles are measured at all AMF1 locations by integrating nephelometers

25 (Uin, 2016a). The size range of the SMPS is around 11 – 465 nm with slightly different ranges

26 for different periods. N_{CCN} is measured at different supersaturations, details are in Table 1. The

27 supersaturations are typically calibrated before and after each campaign at an altitude similar

28 to measurement site by instrument mentors according to CCN handbook (Uin, 2016b). Detailed

29 information about each dataset and measurement site can be found on AOS handbook

Atmospheric
Chemistry
and Physics
Discussions

1   (Jefferson, 2011) or ARM web site (http://www.arm.gov/) and references thereby.

2

3   Ganges Valley (PGH) is located in one of the largest and most rapidly developing sections of

4   the Indian subcontinent. The aerosols in this region have complex sources, including coal and

5   fuel combustion; biomass burning; automobile emissions; and dust. In monsoon seasons, dust

6   dominates the aerosol mass due to transportation (Dumka et al., 2017; Gogoi et al., 2015).

7

8   PVC refers to the on-shore data set for the 'first column' of the Two-Column Aerosol Project

9   (TCAP) on Cape Cod, Massachusetts, USA. This is a marine site but still significantly affected

10   by anthropogenic emissions (Berg et al., 2016).

11

12   MAO refers to Manacapuru in Amazonas, Brazil. Manaus pollution plumes and biomass

13   burning impact the background conditions alternately. During the period we selected for this

14   study, no severe pollution episodes were observed. The σ_{sp} for PM10 never exceeded 250Mm^{-1}

15   in this study.

16

17   Ascension Island (ASI) locates in the southeast Atlantic where westward transport of southern

18   Africa biomass-burning aerosols emphases heavy aerosol loading. Air mass at this site usually

19   a mixture with aged biomass-burning plume and sea-salt aerosol. The aerosol loading can be

20   very low without plume, in this case, there is substantial uncertainty on the backscatter fraction.

21

22   The primary purpose of this study is to use as basic and readily accessible measurement data as

23   possible to estimate N_{CCN}. Aerosol optical properties are measured for different cutoff diameters,

24   usually 1 μm, 2.5 μm, 10 μm or TSP. At several stations there are two sets of AOPs using two

25   cutoff diameters. For this study we chose to use AOP data with the 10 μm cutoff or TSP that

26   are more universally used than smaller cutoff diameters.

27

28   **2.2 Data processing**

29   Regardless of the time resolution of raw data, all the data in this study were adjusted into hourly

Atmospheric
Chemistry
and Physics
Discussions

1   averages before further analyses. Suspicious data within the whole dataset were removed

2   according to the following criteria:

3   1) for the size distribution data, all the data with unexplainable spikes were removed manually;

4   2) for CCN measurements, insufficient water supply may cause underestimation of CCN,

5   especially at lower supersaturation ratios (DMT, 2009). N_{CCN} reading at lower SS% has a

6   sudden drop a few hours before the similar sudden drop for higher SS% under such conditions,

7   so data from such periods were removed;

8   3) if any obvious inconsistencies between the AOPs and PNSD or between the N_{CCN} and PNSD

9   were found on closure study, all the data in the same hour were removed.

10

11   Special treatments were carried out for ASI dataset. There will inevitably be a considerable

12   uncertainty in the backscattering fraction if zero point of either σ_{sp} or σ_{bsp} is inaccurate in very

13   clean conditions. The measured σ_{sp} was in agreement with that calculated from the PNSD with

14   the Mie model. However, in the data σ_{bsp} approaches 0.3 Mm^{-1} whenever σ_{sp} approaches 0. Thus,

15   we subtracted from back scattering coefficients a constant 0.3 Mm^{-1} and no longer used any

16   data points with $\sigma_{sp} < 2$ Mm^{-1} for this site to assure the data quality.

17

18   **2.3 Light scattering calculated from the particle number size distributions**

19   Light scattering coefficients were calculated using the Mie code similar to Bohren and Huffman

20   (1983) for SMEAR II. The refractive index was set to the average value of 1.517+0.019i

21   reported for SMEAR II by Virkkula et al.(2011). The wavelength for Mie modeling was set to

22   550 nm, which is same as in the measurements. The whole size range of the DMPS or the SMPS,

23   depending on the station, was used. The total scattering coefficient (σ_{sp}) and hemispheric

24   backscattering coefficient (σ_{bsp}) represent the scattering phase function integrated over the

25   scattering angles of 0-180° and 90-180°, respectively. The backscatter fraction (BSF) is the

26   ratio between σ_{bsp} and σ_{sp}.

27

1   **2.4 CCN number concentration calculated from the particle number size distribution**

2   Under the assumption of fully internally mixed particles, the CCN number concentration

3   calculated from the particle number size distributions (N_{CCN}(PNSD)) is obtained by integrating

4   the PNSD of particles larger than the critical dry particle diameter (D_m):

5    $$N_{CCN}(PNSD) = \int_{D_m}^{\infty} n(\log D_p) d\log D_p \qquad (1)$$

6   At a given SS. D_m is a diameter above which all particles can act as CCN. For a selected dry

7   diameter of a particle having given hygroscopicity is computed from the maximum of: The

8   Critical Diameter D_m is the minimum dry diameter (D_d) that ensure the κ-Köhler curve (Petters

9   and Kreidenweis, 2007) to have one real solution:

10   $$S(D) = \frac{D^3 - D_d^3}{D^3 - D_d^3(1-\kappa)} \exp\left(\frac{4\sigma_{s/a} M_w}{RT\rho_w D}\right). \qquad (2)$$

11   Here D_d is the dry diameter, $\sigma_{s/a}$ is the surface tension of the solution/air interface, R is the

12   universal gas constant, T is temperature, and D is the diameter of the droplet, ρ_w is the density

13   of water, M_w is the molecular weight of water, and κ is the hygroscopicity parameter. S(D) in

14   this particular case is set to the same supersaturation ratio as CCN being measured (e.g., 0.1%,

15   0.2%, 0.3%, 0.5% and 1.0% for SMEAR II).

16

17   The accuracy of N_{CCN}(PNSD) is affected by the treatment of κ. In this study, we are not trying

18   to achieve an accurate value of κ but instead want to illustrate that even an arbitrary setting of

19   κ can yield reasonable CCN concentrations. This approach is named as 'unknown chemical

20   approach' in (Kammermann et al., 2010) and as 'Prediction of N_{CCN} from the constant κ' in

21   Meng et al., (2014). Both of them give a detailed discussion of how this approach performs.

22   Arbitrary κ is not performing as good as a proper κ when calculating N_{CCN}, yet we believe that

23   it is good enough to be an alternative to measuring CCN in the empirical estimation of this

24   study. Wang et al. (2010) also claimed that N_{CCN}(PNSD) may be successfully obtained by

25   assuming an internal mixture and using bulk composition few hours after emissions. For

26   SORPES, ASI and PVC, we simply set a global-average value of 0.27 for κ (Pringle et al., 2010;

27   Kerminen et al., 2012). For the forest sites, SMEAR II and MAO, we set κ = 0.12, which is

1   close to the value of κ for Aitken mode particles reported previously by studies at forest sites

2   (Sihto et al., 2011; Hong et al., 2014).

3

4   **2.5 Aerosol optical properties and CCN concentrations of simulated size distributions**

5   For studying the relationships of particle size, N_{CCN} and AOPs we generated unimodal particle

6   number size distributions n_{um}(GMD,GSD) with varying the geometric mean diameter (GMD)

7   and geometric standard deviation (GSD). For them we calculated the same AOPs with the Mie

8   model as were obtained from the real measurements from the stations σ_{sp} and σ_{bsp} and from

9   these the BSF at the wavelengths λ = 450, 550 and 700 nm. N_{CCN} was calculated simply by

10   integrating number concentrations of particles larger than a critical diameter of 80 nm, 90 nm,

11   100 nm, and 110 nm.

12

13   **3. Overview of measured properties**

14   At SMEAR II the average values of σ_{sp} at λ =550 nm in PM_1 and PM_{10} were 11.2 and 13.7 Mm^{-}

15   ^{1} and corresponding backscattering fractions were 0.162 and 0.155, respectively, during our

16   study period. These values are consistent with those reported by Virkkula et al. (2011). The

17   average ± standard deviation N_{CCN} was 129 ± 99, 303 ± 228, 391 ± 303, 512 ± 384 and 736 ±

18   492 cm^{-3} at SS% of 0.1, 0.2, 0.3, 0.5 and 1.0%, respectively. The CCN spectrum here did not

19   quite follow the traditional fitting N_{CCN}(CSK) = $C \times$ SS%^{k} (Jefferson 2010, Twomey 1959).

20   One year average–N_{CCN}(CSK) at SMEAR II for SS=0.1% is 197/cm^3, 53% higher than

21   N_{CCN}(mea) for the same period. Also, R^2 of the linear regression between N_{CCN}(CSK) and

22   N_{CCN}(mea) is 0.78 at SS=1.0%, which means that Jefferson's method performs approximately

23   as well for SMEAR II as at the other sites presented by Jefferson (2010). However, our

24   motivation is to develop a method that needs no absorption data.

25

26   **3.1 AOPs and CCN calculated from particle size distributions**

27   Aerosol optical properties calculated from particle number size distributions matched well with

28   the measured scattering coefficients in PM_1. For σ_{sp} larger than about 40 Mm^{-1}, the calculated

29   values were slightly lower than the measured ones. The measured and calculated BSF also

1   matched well with r^2=0.93 for the data with σ_{sp} >10. Another quality check of the CCN data is

2   that the N_{CCN}(PNSD) calculated from *Eq.(1)* was consistent with the measured CCN number

3   concentration N_{CCN}(meas): for the linear regression r^2 was 0.80, 0.91 0.94 and 0.92 for SS=0.1%,

4   0.2%, 0.5% and 1.0%, respectively, and the corresponding slopes varied between 0.85 and ~1.2

5   depending on the value of SS%. The correlation between N_{CCN}(PNSD) and N_{CCN}(meas) was the

6   weakest for the lowest set of supersaturation (0.1%), most probably because the measurement

7   uncertainty is much higher at lower values of SS% compared with higher SS% for DMT CCN

8   counter (Rose et al., 2008).

9

10   **3.2 Relationships between AOPs and CCN**

11   The correlation between N_{CCN} and σ_{sp} was weak at SMEAR II, especially for higher

12   supersaturations (Fig 1). In spite of this, when color-coded with respect to BSF, the relationship

13   between N_{CCN} and σ_{sp} becomes clear: the scatter plot points of N_{CCN} grows almost linearly as a

14   function of σ_{sp} for a narrow range of values of BSF. This indicates BSF can serve as a good

15   proxy for describing the ratio between N_{CCN} and σ_{sp} at SMEAR II.

16

17   Hereafter, we will use the term $R_{CCN/\sigma} = N_{CCN}/\sigma_{sp}$ to describe the relationship between CCN

18   concentration light scattering and similar to Liu and Li (2014). Note that this same ratio was

19   defined as AR_{scat} in Tao et al. (2018). $R_{CCN/\sigma}$ varies over a wide range of values, so a proper

20   parameterization to describe it is of significance.

21

22   **4. Development of the parameterization**

23   **4.1 Site-dependent parameterization for each measured supersaturation, $N_{CCN}(AOP_1)$**

24   The first step in the development of the parameterization was to calculate linear regressions of

25   $R_{CCN/\sigma}$ vs BSF. $R_{CCN/\sigma}$ depends clearly on BSF (Fig. 2) as

26   $$R_{CCN/\sigma} = a \text{ BSF} + b \tag{3}$$

27   At SMEAR II the correlation between BSF and $R_{CCN/\sigma}$ is strong when $\sigma_{sp} > 10$ Mm^{-1}. At $\sigma_{sp} <$

28   10 Mm^{-1} the uncertainty of the nephelometer is higher which may at least partly explain the

29   lower correlation. For each dataset and individual supersaturation, *a* and *b* the slope and offset

Atmospheric
Chemistry
and Physics
Discussions

1   of the linear regressions has a different value as presented in Table 2. The parameterization

2   gives the formula for calculating $N_{CCN}(AOP)$, ie, N_{CCN} calculated from measurements of AOPs:

3    $$N_{CCN}(AOP_1) = (a_{SS\%} * BSF + b_{SS\%}) \cdot \sigma_{sp} \tag{4}$$

4   The subscript 1 for AOP_1 indicates the first set of parameterization.

5

6   Scatter plots of $N_{CCN}(AOP_1)$ vs $N_{CCN}(meas)$ are presented for the supersaturations used at the

7   SMEAR II CCN counter in Fig 3 and for the highest and the lowest SS% used at the other

8   stations in Fig 4. At SMEAR II this approach yields R^2 of 0.70, 0.86, 0.75 and 0.55 for SS=0.1%,

9   0.2%, 0.5% and 1.0%, respectively, and the slopes (and intercepts) are 0.95(13), 0.92(28),

10   0.86(52) and 0.76(87), respectively. All slopes are slightly less than 1 and the intercept are

11   slightly over 0. One explanation is that when both x and y have uncertainties, the least-squares

12   method in the linear regression trend to underestimates the slope (Cantrell, 2008). $N_{CCN}(AOP_1)$

13   overestimates (or underestimates) $N_{CCN}(meas)$ by 4.8%, 1.2%, -4.2% and -12.5% at the above

14   specified supersaturations. For the overall dataset regardless of supersaturations, R^2,

15   slope(intercept) and difference between $N_{CCN}(AOP_1)$ and $N_{CCN}(meas)$ are 0.73, 0.81(56) and -

16   5.1% respectively.

17

18   R^2 between $N_{CCN}(AOP_1)$ and $N_{CCN}(meas)$ is higher at lower supersaturations than at higher

19   supersaturations in most of the scatter plots shown in Figures 3 and 4. The reasonable

20   explanation is that the higher the supersaturation is the smaller are the particles that can act as

21   CCN. The smaller are the particles the less do they contribute to both total scattering and

22   backscattering and the higher is the relative uncertainty of both of them and thus also the

23   uncertainty of $N_{CCN}(AOP_1)$.

24

25   **4.2 General combined parameterization $N_{CCN}(AOP_2)$**

26   In the next step, the slopes and offsets obtained from the linear regression (Table 2) were plotted as

27   a function of SS% (Fig 5). The data obviously depend logarithmically on SS% so that (4) becomes

28   $$N_{CCN}(AOP_2) = \left(a_{ss} BSF + b_{ss} \right) \sigma_{sp} = \left(\left(a_1 \ln(SS\%) + a_0 \right) BSF + b_1 \ln(SS\%) + b_0 \right) \sigma_{sp} \tag{5}$$

29   The coefficients a_0, a_1, b_0 and b_1 obtained from the regression of $a_{SS\%} = a_1 \ln(SS\%) + a_0$ and $b_{SS\%} =$

1     $b_1 \ln(SS\%) + b_0$ for each station are presented in Table 3. The relationships of the coefficients can

2   be used for a combined, more general parameterization. Obviously the a_0 vs. a_1, b_0 vs. b_1, a_1 vs. b_1

3   and b_0 vs. b_0 pairs from all stations follow very accurately same lines (Fig 6). This suggests that

4   there is some underlying reason for it. Linear regressions yielding $a_0 = (2.38 \pm 0.06)a_1$, $b_0 = (2.33 \pm$

5     $0.03)b_1$, and $b_1 = (-0.097 \pm 0.013)a_1 + (6.4 \pm 5.9)$ were used, after the simple algebra in the

6   supplement, to get

7
$$N_{CCN}(AOP_2) \approx \left(\ln(SS\%) + (2.38 \pm 0.06) \right) \left(a_1 (BSF - (0.097 \pm 0.013)) + (6.4 \pm 5.9) \right) \sigma_{sp}$$
$$\approx \ln\left(\frac{SS\%}{0.093 \pm 0.006} \right) \left(a_1 (BSF - (0.097 \pm 0.013)) + (6.4 \pm 5.9) \right) \sigma_{sp} \qquad (6)$$

8   where both the coefficient a_1 and the constant 6.4 ± 5.9 have units of $[N_{CCN}]/[\sigma_{sp}] = cm^{-3}/Mm^{-1}$. This

9   is the general formula for the parameterization. In both (5) and (6) the only unquantified coefficient

10   is now a_1. However, we can find some ways to quantify also it.

11

12   For a given station, if there are simultaneous data of $N_{CCN}(meas)$ and σ_{sp} for some reasonably long

13   period, (6) can be adjusted. Instead of subtracting (0.097 ± 0.013) from BSF the minimum BSF =

14   BSF_{min} in the data set will be used. Further, when $BSF = BSF_{min}$ the factor $a_1(BSF - BSF_{min}) =$

15   0 and $N_{CCN}(AOP_2) \approx R_{min}\sigma_{sp}$ where R_{min} is the minimum $R_{CCN/\sigma}$ in the data set. It follows that

16
$$N_{CCN}(AOP_2) \approx \left(a_1 \ln\left(\frac{SS\%}{0.093 \pm 0.006} \right) (BSF - BSF_{min}) + R_{min} \right) \sigma_{sp} \qquad (7)$$

17   The derivation of (7) is shown in the supplement. In the data processing the 1st percentiles of

18   both BSF and $R_{CCN/\sigma}$ are used as BSF_{min} and R_{min}, respectively. Here the free parameters are a_1,

19   BSF_{min} and R_{min}. The coefficient a_1 is positively correlated with SAE. The linear regressions of a_1

20   and the average and median scattering Ångström exponent of PM_{10} particles (SAE_{10}) (Table 3)   at

21   the 6 sites in the analyzed periods yield $a_1 \approx (298 \pm 51)SAE_{10}$ cm^{-3}/Mm^{-1} and $a_1 \approx (287 \pm 45)SAE_{10}$

22   cm^{-3}/Mm^{-1}, respectively (Fig. 7). The uncertainties are large but, the main point is that the

23   correlations show that a_1 and thus $N_{CCN}(AOP)$ is the higher the higher SAE_{10} is. R_{min} was estimated

24   by calculating the 1st percentile of $R_{CCN/\sigma}$ at each site at each SS%. The average and standard

25   deviation of R_{min} was 5.2 ± 3.3 cm^{-3}/Mm^{-1}. Consequently the parameterization becomes

26
$$N_{CCN}(AOP_2) \approx \left((287 \pm 45)SAE_{10} \cdot \ln\left(\frac{SS\%}{0.093 \pm 0.006} \right) (BSF - BSF_{min}) + (5.2 \pm 3.3) \right) \sigma_{sp} \qquad (8)$$

27

28

Atmospheric
Chemistry
and Physics
Discussions

1 **5. Results and discussion**

2 **5.1 Comparison of N_{CCN} from the AOP parameterization and measurements**

3 The parameterization in *Eq (8)* was applied to the data of the 6 stations and $N_{CCN}(AOP_2)$ was

4 compared with the N_{CCN}(meas) at the supersaturations used in the respective CCN counters.

5 The results are presented as scatter plots of of $N_{CCN}(AOP_2)$ vs. N_{CCN}(meas) (Fig 8a and 8b), the

6 bias of the parameterization calculated as $N_{CCN}(AOP_2)/N_{CCN}$(meas) (Fig 8c) and the squared

7 correlation coefficient R^2 of the linear regression of $N_{CCN}(AOP_2)$ vs. N_{CCN}(meas) (Fig 8d).

8

9 At the site-specific lowest SS% the scatter plots of $N_{CCN}(AOP_2)$ vs. N_{CCN}(meas) of data from

10 most stations get clustered along the 1:1 line, but for the Himalayan site PGH the

11 parameterization yields significantly higher concentrations (Fig 8a). It was mentioned above

12 that we applied also the Jefferson (2010) parameterization to SMEAR II data. At SS=0.1% the

13 average N_{CCN}(CSK) was 53% higher than N_{CCN}(meas) and R^2 of the linear regression was 0.78

14 at SS=1.0%. The bias of our method at SS% = 0.1 was ~0.66 so it underestimated measurements

15 by 34% and $R^2 \approx 0.65$ (Fig 8), lower than that of Jefferson (2010). At SS% > 0.3 the bias varied

16 from 1.1 to 1.3. At the highest SS% the deviations from the 1:1 line are smaller also for PGH

17 (Fig 8b). At PGH at the lowest SS% the bias is > 4 but decreases to ~1.1-1.2 at SS% = 0.4%

18 and even closer to 1 at higher SS%. At SS% > 0.4% the AOP-derived N_{CCN} is higher than the

19 measured concentration at four sites with their bias varying between ~1.1 and ~1.3. For the US

20 coastal site PVC the parameterization constantly underestimates the CCN concentrations by

21 about 30%. For the Amazonian site MAO the bias is close to 1 at the lowest SS% but for the

22 higher SS% it varies from 0.68 to 0.79.

23

24 **5.2 Evaluation of the effect of particle size distribution to the parameterization**

25 The linear relationships of the coefficients of Eq. (5) are so clear (Fig. 6) that there should be

26 some common underlying reason. To study this we generated lognormal unimodal size

27 distributions as explained in section 2.5. GMD was given logarithmically evenly-spaced values

28 from 50 nm to 1600 nm and GSD was given two values: 1.5 representing a relatively narrow

29 size distribution and 2.0 a wide size distribution. We then calculated AOPs, N_{CCN} and $R_{CCN/\sigma}$

1   for these size distributions.

2

3   The reasoning for the approach of estimating N_{CCN} from σ_{sp} and BSF can easily be explained

4   by the similar variations of $R_{CCN/\sigma}$ and BSF (Fig. 9). $R_{CCN/\sigma}$ is the highest for the smallest

5   particles, i.e. for GMD = 50 nm and it decreases with the growing GMD as also BSF. Note that

6   the width of the size distribution has very strong effects on $R_{CCN/\sigma}$: for the wide size distribution

7   it is approximately an order of magnitude lower than for the narrow size distribution.

8

9   Note also that the rates of decrease of $R_{CCN/\sigma}$ and BSF. We used this information for estimating

10   particle sizes with a stepwise linear regression. An example is given by the linear regressions

11   of $R_{CCN/\sigma}$ vs. BSF calculated for 5 consecutive size distributions, first for those that have their

12   GMDs from 50 nm to 100 nm and the second for those that have their GMDs from 100 nm to

13   200 nm (Fig. 10). Note that it is obvious that linear regressions are applicable for short intervals

14   but do not well for the whole size range. The absolute values of the slopes and offsets are clearly

15   lower for the larger particle size range. The particle size that is used for describing the size

16   range of each regression we define here as the equivalent geometric mean diameter GMD_e, the

17   geometric mean of the range of the GMDs of the unimodal size distributions used for each

18   regression. It will be shown below that GMD_e is a mathematical concept helping in explaining

19   the observed relationships, not an actual GMD of the particle size distribution at the sites.

20

21   For the wide size distributions the slopes and offsets of the regressions of $R_{CCN/\sigma}$ vs. BSF

22   decrease and increase, respectively, monotonically with an increasing GMD_e in the whole size

23   range studied here (Fig. 11). For the narrow size distribution the slope decreases to $GMD_e \approx$

24   300 nm and then increases which means there is no unambiguous relationship between them.

25

26   Note also that the ranges of the absolute values of the slopes and offsets of the wide and narrow

27   size distributions are very different. However, they decrease and increase simultaneously. This

28   is the link to the observations from the field stations. We plotted the offset. vs slope of the

29   unimodal size distributions and those obtained from the linear regressions of the field data at

14

Atmospheric
Chemistry
and Physics
Discussions

1   the supersaturatios presented in Table 2 and below it the GMD_e vs. the slopes of the regressions

2   of the unimodal size distributions (Fig 12). In Fig. 12 also the effect of the choice of the

3   activation diameters of 80 nm, 90 nm, and 110 nm is shown.

4

5   Several observations can be made of Fig. 12. First, for the simulated wide size distributions the

6   relationship of the offset and slope is unambiguous but not for the narrow size distributions at

7   sizes $GMD_e > \sim 200$ nm (Fig 12b). Secondly, the field data points obviously follow the lines of

8   the simulations. This supports the approach for the interpretation of the relationships presented

9   above (Fig. 6) for the coefficients in Eq. (5). Especially, note the similar ranges of b_0 vs a_0 in

10   Fig 6d and the ranges of b vs a in Fig 12a. This is the link to Eq. (5): if we set SS% = 1, the

11   equation reduces to $N_{CCN} = (a_0 BSF + b_0)\sigma_{sp}$. Together with the clear linear relationships between

12   the coefficients this suggests that the coefficients of Eq. (5) depend on the GMD and GSD of

13   the particle size distributions.

14

15   Most field data agree well with the b vs. a line of the unimodal wide size distribution with the

16   lowest activation diameter of 80 nm. For instance, the PVC data point corresponding to the

17   highest supersaturation has the highest slope (1970 cm^{-3}/Mm^{-3}, Table 2) and it is close to the

18   above-mentioned line (Fig. 12a). The corresponding GMD_e of the unimodal size distribution is

19   also ~80 nm (Fig 12b). The SMEAR II high SS% offset vs. slope fits best with the

20   corresponding lines of the narrow unimodal size distributions with all activation diameters and

21   the corresponding $GMD_e \approx 150 - 180$ nm.

22

23   At the lowest SS% the offset vs. slope points of all stations agree with the lines derived from

24   the lines derived from the unimodal modes. This is interesting considering the high

25   uncertainties involved in the regressions at the lowest SS% (Fig. 2). For ASI the slopes and

26   offsets of the lowest and highest SS% are especially close to each other, closer than at any other

27   station (Fig. 12a), and the corresponding $GMD_e \approx 750$ nm and 400 nm, respectively, when the

28   GMD_e vs. a relationship of any of the wide distributions is used (Fig. 12b). For PGH at the

29   lowest SS% the slope is actually negative which is not obtained from the simulations at all so

Atmospheric
Chemistry
and Physics
Discussions

1   no GMD$_e$ cannot be given for it.

2

3   **5.3 Aerosol size characteristics for all site**

4   As it was shown above, particle size distributions affect the coefficients of the parameterization. It

5   is therefore discussed here how the size distributions vary at the six sites of the study and whether

6   they support the interpretations presented above. The size distributions are discussed using the

7   particle number size distribution and the ratios of σ_{sp} of PM$_1$ and PM$_{10}$ size ranges data from those

8   stations where they are available.

9

10

11   **5.3.1 Diurnal variation of particle number size distribution**

12   Fig. 13a shows the averaged diurnal cycle of PNSD at the sites where either a DMPS or SMPS is

13   available. New particle formation (NPF) events is a significant source of uncertainty in the

14   prediction of N$_{CCN}$ (Kerminen et al., 2012; Ma et al., 2016). Complete NPF events start from a

15   burst of sub 10 nm particles and continuous growing up to a few hundred nanometers. As a result,

16   the size distribution varies significantly. NPF is one possible explanation of the poor N$_{CCN}$-σ_{sp}

17   correlation.

18

19   SMEAR II and SORPES are reported to have an appreciable frequency of NPF (Kulmala et al.,

20   2004; Dal Maso et al., 2005; Sihto et al., 2006; Qi et al., 2015). Continuous growth in particle size

21   at SORPES can usually last for several days after NPF (Shen et al. 2018). Similar growth patterns

22   have also been observed in the Two-Column Aerosol Project (TCAP; http://campaign.arm.gov/tcap/;

23   refers as PVC in this study) according to Kassianov et al. (2014). NPF is rarely observed in the

24   Amazon forest where MAO is located. However, it does take place also at MAO as is shown in the

25   diurnal cycle of PNSD. At ASI, there no evidence of NPF according to the PNSD diurnal cycle.

26

27   These observations of the NPF are compared with the bias and correlation coefficients of the

28   parameterization discussed in section 5.1 (Fig. 8). The correlation coefficient of N$_{CCN}$(AOP$_2$) vs.

29   N$_{CCN}$(meas) is the highest, R$^2 \approx 0.8$ at all SS% at ASI where no NPF takes place and clearly lower

Atmospheric
Chemistry
and Physics
Discussions

1 at the other sites (Fig 8d). For the bias NPF appears not to have a clear influence: for both SMEAR

2 II and SORPES bias varies from ~1.1 to ~1.4 at SS% > 0.1%.

3

4 **5.3.2 Distribution of geometric mean diameter**

5 Figure 13b presents the normalized distribution of the geometric mean diameter at SMEAR II,

6 SORPES, PVC, MAO and ASI. It varies from 20 nm to 200 nm at all sites, with the most

7 frequent GMD between ~70 nm and ~120 nm depending on the site. This shows clearly that

8 the above-presented equivalent geometric mean diameter GMD_e calculated assuming a

9 unimodal size distribution is not a quantitative GMD of the size distribution, it is a mathematical

10 concept that explains partially the relationships of $R_{CCN/\sigma}$ and BSF.

11

12 The frequency distribution of GMD at SMEAR II is the widest among five sites with PNSD data

13 available, followed by SORPES and PVC. At MAO the frequency distribution of GMD has two

14 peaks in this study, different from that at ATTO in Amazonas (Schmale et al., 2018)). The lower

15 peak is possibly due to the burst of sub-20 nm particles since they have little chance to grow to sizes

16 that can serve as CCN. The second peak around 100 nm possibly represents the GMD without the

17 burst of sub-20 nm particles and it is distinctly narrower than at SMEAR II, SORPES and PVC.

18

19 A comparison of the correlation coefficients of $N_{CCN}(AOP_2)$ vs. $N_{CCN}(meas)$ (Fig. 8) and the widths

20 of the GMD frequency distributions (Fig. 13b) does not show any clear relationships between them,

21 other than that of ASI. The frequency distribution of GMD is the narrowest at ASI indicating that

22 the average particle size does not change much throughout the whole period. This is in line with the

23 low variation of the slope and offset of the R_{CCN} vs BSF of ASI (Fig 12a). At ASI also the correlation

24 coefficient of $N_{CCN}(AOP_2)$ vs. $N_{CCN}(meas)$ is the highest, $R^2 \approx 0.8$ at all SS%.

25

26 **5.3.3 Contribution of light scattering by sub-µm particles**

27 There is one more measure related to particle size distribution, the ratio between σ_{sp} of sub-1 µm

28 and sub-10 µm aerosol ($\sigma_{sp}(PM_1)/\sigma_{sp}(PM_{10})$). At SMEAR II, the contribution of submicron particles

29 usually varies within range 0.8~0.9 and it is the highest among all sites in this study. PVC has two

Atmospheric
Chemistry
and Physics
Discussions

1   peaks in the $\sigma_{sp}(PM_1)/\sigma_{sp}(PM_{10})$ distribution, the peak around 0.2 corresponds to air masses from

2   the sea, with a very low scattering coefficient and N_{CCN}. By ignoring the cleanest air masses ($\sigma_{sp}<5$

3   Mm^{-1}), the fraction of $\sigma_{sp}(PM_1)/\sigma_{sp}(PM_{10})$ is usually around 0.8, which is just slightly lower than at

4   SMEAR II. At PGH and MAO, the distribution of the ratio is wider, and the peak position is around

5   0.65. The overall contribution of sub-μm particle light scattering at PGH is moderate among the

6   sites in this study. At ASI $\sigma_{sp}(PM_1)/\sigma_{sp}(PM_{10})$ is the lowest among all sites in this study, indicating

7   that particles larger than 1 μm contribute a considerable fraction of light scattering. For SORPES

8    $\sigma_{sp}(PM_1)/\sigma_{sp}(PM_{10})$ is not available.

9

10   Among those five sites, when $\sigma_{sp}(PM_1)/\sigma_{sp}(PM_{10})$ decreases, the correlation between BSF and

11    $R_{CCN/\sigma}$ decreases. At some sites (e.g., ASI) the BSF of PM_{10} is often be even larger than that of PM_1

12   which is most probably an error in the measurements but it may also be due to non-spherical

13   particles like sea salt and dust, which will blur the correlation between BSF and $R_{CCN/\sigma}$. In such a

14   case the increase of the amount of large particles leads to an increase of BSF and a decrease of

15    $R_{CCN/\sigma}$ which is opposite to the usual positive correlation between BSF and $R_{CCN/\sigma}$ in this study.

16   Thus, the lower $\sigma_{sp}(PM_1)/\sigma_{sp}(PM_{10})$ may in principle result in a poor performance of our method.

17   However, a comparison of the correlation coefficients and the $\sigma_{sp}(PM_1)/\sigma_{sp}(PM_{10})$ frequency

18   distributions of each site shows the opposite. At the highest SS% of each site the R^2 in a decreasing

19   order is ASI, PGH, MAO, SORPES, SMEAR II, and PVC (Fig. 8d). The peaks of the frequency

20   distribution of $\sigma_{sp}(PM_1)/\sigma_{sp}(PM_{10})$ are, in a growing order, ASI: 0.375, PGH: 0.625, MAO: 0.65,

21   PVC: 0.825, SMEAR II: 0.875. Note that at SORPES there is only one size range measured. Of

22   these only PVC and SMEAR II are not in the same order. On the other hand, the bias at the highest

23   SS% has no clear relationship with $\sigma_{sp}(PM_1)/\sigma_{sp}(PM_{10})$: for MAO our parameterization

24   underestimates the N_{CCN} the most (bias ≈ 0.68) and for ASI it overestimates the most (bias ≈ 1.28).

25

26   **6. Conclusions**

27   The relationships between aerosol optical properties, CCN number concentrations (N_{CCN}) and

28   particle number size distributions were investigated based on in-situ measurement data from

29   six stations in very different environments around the world. The goal of the work was to find

1 a parametrization to obtain N_{CCN} from sites where AOPs are measured but no CCN counter is

2 available.

3

4 There are many previous parameterizations for doing just the same. As a starting point we used the

5 parameterization presented by Jefferson (2010). That one needs also absorption measurements since

6 it includes single-scattering albedo. We instead studied how the parameterization would look like if

7 only total scattering and backscattering data were available.

8

9 The basic idea for the parameterization is that N_{CCN} is proportional to σ_{sp} and a function of the

10 backscatter fraction (BSF), as is also in the parameterization of Jefferson (2010). One clear

11 difference is that our data analysis showed that the dependence on supersaturation is logarithmic,

12 different from that of Jefferson (2010). Actually this result is qualitatively in line with the

13 relationship between AOD and CCN reported by Andreae (2010).

14

15 The coefficients of the parameterization derived for the different sites showed that they appear

16 to be linearly related to each other. A simulation with unimodal size distributions showed that

17 the relationships are affected by the size and width of the size distribution and the activation

18 diameter.

19

20 We were able to derive a parameterization that describes all sites. The parameterization not only

21 depends on BSF but also on the wavelength dependency of scattering, i.e. the scattering

22 Ångström exponent SAE. Further studies need to be done to compare different

23 parameterizations for data from various different sites.

24

25 **Author contributions**

26 YS carried out measurements at SORPES in China, analyzed and visualized data of all sites, and

27 wrote the original draft. AV contributed to data analysis and visualization, writing and editing the

28 original draft, and supervised the work of YS in Finland. AD provided funding for the measurements

29 and research at SORPES in China, acquired funding for YS in China, and supervised the work of

Atmospheric
Chemistry
and Physics
Discussions

1 YS. KL, HK and PA carried out measurements, data collection and maintenance of measurement

2 data of SMEAR II in Finland. YS, XC, XQ, WN and XH carried out measurements, data collection

3 and maintenance of measurement data of SORPES in China. MK and TP provided the funding for

4 YS in Finland. MK provided funding for the measurements and research at SMEAR II in Finland.

5 TP and VMK formulated the goals of the research and supervised it.

6

17

18 **References**

19 Aalto, P., Hämeri, K., Becker, E., Weber, R., Salm, J., Mäkelä, J., Hoell, C., O'dowd, C.,

20 Hansson, H.-C., Väkevä, M., Koponen, I., Buzorius, G., and Kulmala, M.: Physical

21 characterization of aerosol particles during nucleation events, Tellus B, 53, 344–358,

22 https://doi.org/10.3402/tellusb.v53i4.17127, 2001.

23

24 Andreae, M. O.: Correlation between cloud condensation nuclei concentration and aerosol

25 optical thickness in remote and polluted regions, Atmos. Chem. Phys., 9, 543–556,

26 https://doi.org/10.5194/acp-9-543-2009, 2009.

27

28 Berg, L. K., Fast, J. D., Barnard, J. C., Burton, S. P., Cairns, B., Chand, D., Comstock, J. M.,

29 Dunagan, S., Ferrare, R. A., Flynn, C. J., Hair, J. W., Hostetler, C. A., Hubbe J., Jefferson, A.,

1   Johnson, R., Kassianov, E. I., Kluzek, C. D., Kollias, P., Lamer, K., Lantz, K., Mei, F., Miller,

2   M. A., Michalsky, J., Ortega, I., Pekour, M., Rogers, R. R., Russell, P. B., Redemann, J.,

3   Sedlacek III, A. J., Segal-Rosenheimer, M., Schmid, B., Shilling, J. E., Shinozuka, Y.,

4   Springston, S. R., Tomlinson, J. M., Tyrrell, M., Wilson, J. M., Volkamer, R., Zelenyuk, A., and

5   Berkowitz, C. M.: The Two-Column Aerosol Project: Phase I – Overview and impact of

6   elevated aerosol layers on aerosol optical depth, J. Geophys. Res.-Atmos., 121, 336–361, 2016.

7

8   Bohren, C. F. and Huffman, D. R.: Absorption and scattering of light by small particles, 1st ed.

9   Wiley, New York, 57–81, 1983.

10

11   Cantrell, C. A.: Technical Note: Review of methods for linear leastsquares fitting of data and

12   application to atmospheric chemistry problems, Atmos. Chem. Phys., 8, 5477–5487,

13   doi:10.5194/acp-8-5477-2008, 2008.

14

15   Crosbie, E., Youn, J.-S., Balch, B., Wonaschütz, A., Shingler, T., Wang, Z., Conant, W. C.,

16   Betterton, E. A., and Sorooshian, A.: On the competition among aerosol number, size and

17   composition in predicting CCN variability: a multi-annual field study in an urbanized desert,

18   Atmos. Chem. Phys., 15, 6943-6958, https://doi.org/10.5194/acp-15-6943-2015, 2015.

19

20   Dal Maso, M., Kulmala, M., Riipinen, I., Wagner, R., Hussein, T., Aalto, P. P., and Lehtinen, K.

21   E. J.: Formation and growth of fresh atmospheric aerosols: eight years of aerosol size

22   distribution data from SMEAR II, Hyytiälä, Finland, Boreal Environ. Res., 10, ¨ 323–336, 2005

23

24   Ding, A. J., Fu, C. B., Yang, X. Q., Sun, J. N., Zheng, L. F., Xie, Y. N., Herrmann, E., Nie, W.,

25   Petäjä, T., Kerminen, V.-M., and Kulmala, M.: Ozone and fine particle in the western Yangtze

26   River Delta: an overview of 1 yr data at the SORPES station, Atmos. Chem. Phys., 13, 5813–

27   5830, doi:10.5194/acp-13-5813- 2013, 2013.

28

29   Ding, A. J., Nie, W., Huang, X., Chi, X., Sun, J., Kerminen, V. M., Xu, Z., Guo, W., Petaja, T.,

1 Yang, X. Q., Kulmala, M., and Fu, C.: Long-term observation of air pollution-weather/climate

2 interactions at the SORPES station: A review and outlook, Front. Environ. Sci. Eng., 10,

3 doi:10.1007/s11783-016-0877-3, online first, 2016.

4

5 DMT: Cloud Condensation Nuclei Counter Operator Manual, DOC-0086 Rev G-1, Droplet

6 Measurement Technologies, Inc., p. 107, 2009

7

8 Dusek, U., Frank, G. P., Hildebrandt, L, Curtius, J., Schneider, J., Walter, S., Chand, D.,

9 Drewnick, F., Hings, S., Jung, D., Bormann, S., and Andreae, M. O.: Size matters more than

10 chemistry for cloud-nucleating ability of aerosol particles, Science, 312, 1375–1378, 2006.

11

12 Ervens, B., Cubison, M., Andrews, E., Feingold, G., Ogren, J. A., Jimenez, J. L., DeCarlo, P.,

13 and Nenes, A.: Prediction of cloud condensation nucleus number concentration using

14 measurements of aerosol size distributions and composition and light scattering enhancement

15 due to humidity, J. Geophys. Res.-Atmos., 112, D10S32, https://doi.org/10.1029/2006jd007426,

16 2007.

17

18 Forster, P., Ramaswamy, V., Artaxo, P., Berntsen, T., Betts, R., Fahey, D. W., Haywood, J., Lean,

19 J., Lowe, D. C., Myhre, G., Nganga, J., Prinn, R., Raga, G., Schulz, M., and Van Dorland, R.:

20 Changes in Atmospheric Constituents and in Radiative Forcing, in: Climate Change 2007: The

21 Physical Science Basis, contribution of Working Group I to the Fourth Assessment Report of

22 the Intergovernmental Panel on Climate Change, edited by: Solomon, S. D., Qin, M., Manning,

23 Z., Chen, M., Marquis, K. B., Averyt, M. T., and Miller, H. L., Cambridge University Press,

24 Cambridge, United Kingdom and New York, NY, USA, 129– 134, 2007.

25

26 Ghan, S. J., Rissman, T. A., Elleman, R., Ferrare, R. A., Turner, D., Flynn, C., Wang, J., Ogren,

27 J., Hudson, J., Jonsson, H. H., VanReken, T., Flagan, R. C., and Seinfeld, J. H.: Use of in situ

28 cloud condensation nuclei, extinction, and aerosol size distribution measurements to test a

29 method for retrieving cloud condensation nuclei profiles from surface measurements, J.

Atmospheric
Chemistry
and Physics
Discussions

1   Geophys. Res.- Atmos., 111, D05s10, https://doi.org/10.1029/2004jd005752, 2006.

2

3   Gogoi, M. M., S. S. Babu, V. Jayachandran, K. K. Moorthy, S. K. Satheesh, M. Naja, and V.

4   R. Kotamarthi (2015), Optical properties and CCN activity of aerosols in a high-altitude

5   Himalayan environment: Results from RAWEX-GVAX, J. Geophys. Res. Atmos., 120, 2453–

6   2469, doi:10.1002/2014JD022966.

7

8   Hong, J., Häkkinen, S. A. K., Paramonov, M., Äijälä, M., Hakala, J., Nieminen, T., Mikkilä, J.,

9   Prisle, N. L., Kulmala, M., Riipinen, I., Bilde, M., Kerminen, V.-M., and Petäjä, T.:

10 Hygroscopicity, CCN and volatility properties of submicron atmospheric aerosol in a boreal

11 forest environment during the summer of 2010, Atmos. Chem. Phys., 14, 4733-4748,

12 https://doi.org/10.5194/acp-14-4733-2014, 2014.

13

14 Hudson, J. G.: Cloud condensation nuclei, J. Appl. Meteorol., 32, 596–607, 1993.

15

16 Hudson, J. G.: Variability of the relationship between particle size and cloud-nucleating ability,

17 Geophys. Res. Lett., 34, 08801, doi:10.1029/2006GL028850, 2007.

18

19 Jefferson, A.: Empirical estimates of CCN from aerosol optical properties at four remote sites,

20 Atmos. Chem. Phys., 10, 6855-6861, https://doi.org/10.5194/acp-10-6855-2010, 2010.

21

22 Jefferson, A.: Aerosol observing system (AOS) handbook, ARMTR-014, US Dep. of Energy,

23 Washington, D. C., 2011

24

25 Kammermann, L., Gysel, M., Weingartner, E., Herich, H., Cziczo, D. J., Holst, T.,

26 Svenningsson, B., Arneth, A., and Baltensperger, U.: Sub-arctic atmospheric aerosol

27 composition 3: Measured and modeled properties of cloud condensation nuclei (CCN), J.

28 Geophys. Res., 115, D04202, doi:10.1029/2009JD012447, 2010.

29

1   Kassianov, E., Barnard, J., Pekour, M., Berg, L. K., Shilling, J., Flynn, C., Mei, F., and Jefferson,

2   A.: Simultaneous retrieval of effective refractive index and density from size distribution and

3   light-scattering data: weakly absorbing aerosol, Atmos. Meas. Tech., 7, 3247-3261,

4   https://doi.org/10.5194/amt-7-3247-2014, 2014.

5

6   Kerminen, V.-M., Paramonov, M., Anttila, T., Riipinen, I., Fountoukis, C., Korhonen, H., Asmi,

7   E., Laakso, L., Lihavainen, H., Swietlicki, E., Svenningsson, B., Asmi, A., Pandis, S. N.,

8   Kulmala, M., and Petäjä, T.: Cloud condensation nuclei production associated with atmospheric

9   nucleation: a synthesis based on existing literature and new results, Atmos. Chem. Phys., 12,

10 12037-12059, https://doi.org/10.5194/acp-12-12037-2012, 2012.

11

12 Kuang, C.: TSI Model 3936 Scanning Mobility Particle Spectrometer Instrument Handbook,

13 United States, doi:10.2172/1245993, https://www.osti.gov/servlets/purl/1245993, 2016.

14

15 Kulmala, M., Laaksonen, A., Korhonen, P., Vesala, T., Ahonen, T., and Barrett, J. C.: The effect

16 of atmospheric nitric acid vapor on cloud condensation nuclei activation, J. Geophys. Res., 98,

17 22949–22958, 1993.

18

19 Kulmala, M., Vehkamäki, H., Petäjä, T., Dal Maso, M., Lauri, A., Kerminen, V.M., Birmili, W.

20 and McMurry, P.H.: Formation and growth rates of ultrafine atmospheric particles: A review of

21 observations, J. Aerosol Sci., 35, 143–176, 2004

22

23 Liu, J. and Li, Z.: Estimation of cloud condensation nuclei concentration from aerosol optical

24 quantities: influential factors and uncertainties, Atmos. Chem. Phys., 14, 471–483,

25 https://doi.org/10.5194/acp-14-471-2014, 2014.

26

27 Luoma, K., Virkkula, A., Aalto, P., Petäjä, T., and Kulmala, M.: Over a ten-year record of

28 aerosol optical properties at SMEAR II, Atmos. Chem. Phys. Discuss.,

29 https://doi.org/10.5194/acp-2018-981, in review, 2018.

Atmospheric
Chemistry
and Physics
Discussions

1

2   Ma, N., Birmili, W., Müller, T., Tuch, T., Cheng, Y. F., Xu, W. Y., Zhao, C. S., and Wiedensohler,

3   A.: Tropospheric aerosol scattering and absorption over central Europe: a closure study for the

4   dry particle state, Atmos. Chem. Phys., 14, 6241-6259, https://doi.org/10.5194/acp-14-6241-

5   2014, 2014.

6

7   Ma, N., Zhao, C., Tao, J., Wu, Z., Kecorius, S., Wang, Z., Größ, J., Liu, H., Bian, Y., Kuang, Y.,

8   Teich, M., Spindler, G., Müller, K., van Pinxteren, D., Herrmann, H., Hu, M., and Wiedensohler,

9   A.: Variation of CCN activity during new particle formation events in the North China Plain,

10   Atmos. Chem. Phys., 16, 8593-8607, https://doi.org/10.5194/acp-16-8593-2016, 2016.

11

12   Mather, J. H. and Voyles, J. W.: The Arm Climate Research Facility: A Review of Structure and

13   Capabilities, Bull. Amer. Meteor. Soc., 94, 377–392, 2013.

14

15   Meng, J. W., Yeung, M. C., Li, Y. J., Lee, B. Y. L., and Chan, C. K.: Size-resolved cloud

16   condensation nuclei (CCN) activity and closure analysis at the HKUST Supersite in Hong Kong,

17   Atmos. Chem. Phys., 14, 10267-10282, https://doi.org/10.5194/acp-14-10267-2014, 2014.

18

19   Paramonov , M , Kerminen , V -M , Gysel , M , Aalto , P P , Andreae , M O , Asmi , E ,

20   Baltensperger , U , Bougiatioti , A , Brus , D , Frank , G P , Good , N , Gunthe , S S , Hao , L ,

21   Irwin , M , Jaatinen , A , Juranyi , Z , King , S M , Kortelainen , A , Kristensson , A , Lihavainen ,

22   H , Kulmala , M , Lohmann , U , Martin , S T , McFiggans , G , Mihalopoulos , N , Nenes , A ,

23   O'Dowd , C D , Ovadnevaite , J , Petaja , T , Poschl , U , Roberts , G C , Rose , D , Svenningsson ,

24   B , Swietlicki , E , Weingartner , E , Whitehead , J , Wiedensohler , A , Wittbom , C & Sierau ,

25   B 2015 , ' A synthesis of cloud condensation nuclei counter (CCNC) measurements within the

26   EUCAARI network ' Atmospheric Chemistry and Physics , vol. 15 , no. 21 , pp. 12211-12229 .

27   https://doi.org/10.5194/acp-15-12211-2015.

28

29   Petters, M. D., and S. M. Kreidenweis, S. M.: A single parameter representation of hygroscopic

1 growth and cloud condensation nucleus activity Atmos. Chem. Phys., 7, 1961–1971,

2 doi:10.5194/acp-7-1961-2007, 2007.

3

4 Pringle, K. J., Tost, H., Pozzer, A., Pöschl, U., and Lelieveld, J.: Global distribution of the

5 effective aerosol hygroscopicity parameter for CCN activation, Atmos. Chem. Phys., 10, 5241-

6 5255, https://doi.org/10.5194/acp-10-5241-2010, 2010.

7

8 Pöhlker, M. L., Pöhlker, C., Ditas, F., Klimach, T., Hrabe de Angelis, I., Araújo, A., Brito, J.,

9 Carbone, S., Cheng, Y., Chi, X., Ditz, R., Gunthe, S. S., Kesselmeier, J., Könemann, T., Lavrič,

10 J. V., Martin, S. T., Mikhailov, E., Moran-Zuloaga, D., Rose, D., Saturno, J., Su, H., Thalman,

11 R., Walter, D., Wang, J., Wolff, S., Barbosa, H. M. J., Artaxo, P., Andreae, M. O., and Pöschl,

12 U.: Long-term observations of cloud condensation nuclei in the Amazon rain forest – Part 1:

13 Aerosol size distribution, hygroscopicity, and new model parametrizations for CCN prediction,

14 Atmos. Chem. Phys., 16, 15709-15740, https://doi.org/10.5194/acp-16-15709-2016, 2016.

15

16 Qi, X. M., Ding, A. J., Nie, W., Petäjä, T., Kerminen, V.-M., Herrmann, E., Xie, Y. N., Zheng,

17 L. F., Manninen, H., Aalto, P., Sun, J. N., Xu, Z. N., Chi, X. G., Huang, X., Boy, M., Virkkula,

18 A., Yang, X.-Q., Fu, C. B., and Kulmala, M.: Aerosol size distribution and new particle

19 formation in the western Yangtze River Delta of China: 2 years of measurements at the

20 SORPES station, Atmos. Chem. Phys., 15, 12445-12464, https://doi.org/10.5194/acp-15-

21 12445-2015, 2015.

22

23 Rose, D., Gunthe, S. S., Mikhailov, E., Frank, G. P., Dusek, U., Andreae, M. O., and Pöschl, U.:

24 Calibration and measurement uncertainties of a continuous-flow cloud condensation nuclei

25 counter (DMT-CCNC): CCN activation of ammonium sulfate and sodium chloride aerosol

26 particles in theory and experiment, Atmos. Chem. Phys., 8, 1153-1179,

27 https://doi.org/10.5194/acp-8-1153-2008, 2008.

28

29 Schmale, J., Henning, S., Henzing, B., Keskinen, H., Sellegri, K., Ovadnevaite, J., Bougiatioti,

1   A., Kalivitis, N., Stavroulas, I., Jefferson, A., Park, M., Schlag, P., Kristensson,

2   A., Iwamoto, Y., Pringle, K., Reddington, C., Aalto, P., Äijälä, M.,

3   Baltensperger, U., Bialek, J., Birmili, W., Bukowiecki, N., Ehn, M., Fjæraa, A. M., Fiebig,

4   M., Frank, G., Fröhlich, R., Frumau, A., Furuya, M., Hammer, E., Heikkinen, L., Herrmann, E.,

5   Holzinger, R., Hyono, H., Kanakidou, M., Kiendler-Scharr, A., Kinouchi, K., Kos, G., Kulmala,

6   M., Mihalopoulos, N., Motos, G., Nenes, A., O'Dowd, C., Paramonov, M., Petäjä, T., Picard,

7   D., Poulain, L., Prévôt, A. S. H., Slowik, J., Sonntag, A., Swietlicki, E., Svenningsson, B.,

8   Tsurumaru, H., Wiedensohler, A., Wittbom, C., Ogren, J. A., Matsuki, A., Yum, S. S., Myhre,

9   C. L., Carslaw, K., Stratmann, F. and Gysel, M.: Collocated observations of cloud

10 condensation nuclei, particle size distributions, and chemical composition, Sci.

11 Data, 4, 170003, doi:10.1038/sdata.2017.3, 2017a.

12

13 Schmale, J., Henning, S., Decesari, S., Henzing, B., Keskinen, H., Sellegri, K., Ovadnevaite, J.,

14 Pöhlker, M. L., Brito, J., Bougiatioti, A., Kristensson, A., Kalivitis, N., Stavroulas, I., Carbone,

15 S., Jefferson, A., Park, M., Schlag, P., Iwamoto, Y., Aalto, P., Äijälä, M., Bukowiecki, N., Ehn,

16 M., Frank, G., Fröhlich, R., Frumau, A., Herrmann, E., Herrmann, H., Holzinger, R., Kos, G.,

17 Kulmala, M., Mihalopoulos, N., Nenes, A., O'Dowd, C., Petäjä, T., Picard, D., Pöhlker, C.,

18 Pöschl, U., Poulain, L., Prévôt, A. S. H., Swietlicki, E., Andreae, M. O., Artaxo, P.,

19 Wiedensohler, A., Ogren, J., Matsuki, A., Yum, S. S., Stratmann, F., Baltensperger, U., and

20 Gysel, M.: Long-term cloud condensation nuclei number concentration, particle number size

21 distribution and chemical composition measurements at regionally representative observatories,

22 Atmos. Chem. Phys., 18, 2853-2881, https://doi.org/10.5194/acp-18-2853-2018, 2018.

23

24 Schwartz, S. E., Charlson, R. J., Kahn, R. A., Ogren, J. A., and Rodhe, H.: Why hasn't Earth

25 warmed as much as expected?, J. Climate, 23, 2453–2464, 2010.

26

27 Shen, Y., Virkkula, A., Ding, A., Wang, J., Chi, X., Nie, W., Qi, X., Huang, X., Liu, Q., Zheng,

28 L., Xu, Z., Petäjä, T., Aalto, P. P., Fu, C., and Kulmala, M.: Aerosol optical properties at

29 SORPES in Nanjing, east China, Atmos. Chem. Phys., 18, 5265-5292,

1   https://doi.org/10.5194/acp-18-5265-2018, 2018.

2

3   Shinozuka, Y., Clarke, A. D., DeCarlo, P. F., Jimenez, J. L., Dunlea, E. J., Roberts, G. C.,

4   Tomlinson, J. M., Collins, D. R., Howell, S. G., Kapustin, V. N., McNaughton, C. S., and Zhou,

5   J.: Aerosol optical properties relevant to regional remote sensing of CCN activity and links to

6   their organic mass fraction: airborne observations over Central Mexico and the US West Coast

7   during MILAGRO/INTEX-B, Atmos. Chem. Phys., 9, 6727-6742, https://doi.org/10.5194/acp-

8   9-6727-2009, 2009.

9

10   Shinozuka, Y., Clarke, A. D., Nenes, A., Jefferson, A., Wood, R., McNaughton, C. S., Ström,

11   J., Tunved, P., Redemann, J., Thornhill, K. L., Moore, R. H., Lathem, T. L., Lin, J. J., and Yoon,

12   Y. J.: The relationship between cloud condensation nuclei (CCN) concentration and light

13   extinction of dried particles: indications of underlying aerosol processes and implications for

14   satellitebased   CCN   estimates,   Atmos.   Chem.   Phys.,   15,   7585–7604,

15   https://doi.org/10.5194/acp-15-7585-2015, 2015

16

17   Sihto, S.-L., Kulmala, M., Kerminen, V.-M., Dal Maso, M., Petäjä, T., Riipinen, I., Korhonen,

18   H., Arnold, F., Janson, R., Boy, M., Laaksonen, A., and Lehtinen, K. E. J.: Atmospheric

19   sulphuric acid and aerosol formation: implications from atmospheric measurements for

20   nucleation   and   early   growth   mechanisms,   Atmos.   Chem.   Phys.,   6,   4079-4091,

21   https://doi.org/10.5194/acp-6-4079-2006, 2006.

22

23   Sihto, S.-L., Mikkila, J., Vanhanen, J., Ehn, M., Liao, L., Lehtipalo, ¨ K., Aalto, P. P., Duplissy,

24   J., Petaj¨ a, T., Kerminen, V.-M., Boy, ¨ M., and Kulmala, M.: Seasonal variation of CCN

25   concentrations and aerosol activation properties in boreal forest, Atmos. Chem. Phys., 11,

26   13269–13285, doi:10.5194/acp-11-13269-2011, 2011.

27

28   Tao, J., Zhao, C., Kuang, Y., Zhao, G., Shen, C., Yu, Y., Bian, Y., and Xu, W.: A new method

29   for calculating number concentrations of cloud condensation nuclei based on measurements of

Atmospheric
Chemistry
and Physics
Discussions

1   a three-wavelength humidified nephelometer system, Atmos. Meas. Tech., 11, 895-906,

2   https://doi.org/10.5194/amt-11-895-2018, 2018.

3

4   Twomey, S.: The influence of cloud nucleus population on the microstructure and stability of

5   convective clouds, Tellus, 11, 408– 411, 1959.

6

7   Uin, J.: Integrating Nephelometer Instrument Handbook, United States. doi:10.2172/1246075.

8   https://www.osti.gov/servlets/purl/1246075, 2016a

9

10   Uin, J.: Cloud Condensation Nuclei Particle Counter (CCN) Instrument Handbook, United

11   States. doi:10.2172/1251411. https://www.osti.gov/servlets/purl/1251411, 2016b

12

13   Virkkula, A., Backman, J., Aalto, P. P., Hulkkonen, M., Riuttanen, L., Nieminen, T., dal Maso,

14   M., Sogacheva, L., de Leeuw, G., and Kulmala, M.: Seasonal cycle, size dependencies, and

15   source analyses of aerosol optical properties at the SMEAR II measurement station in Hyytiälä,

16   Finland, Atmos. Chem. Phys., 11, 4445-4468, https://doi.org/10.5194/acp-11-4445-2011, 2011.

17

18   Wang, J., Cubison, M. J., Aiken, A. C., Jimenez, J. L., and Collins, D. R.: The importance of

19   aerosol mixing state and size-resolved composition on CCN concentration and the variation of

20   the importance with atmospheric aging of aerosols, Atmos. Chem. Phys., 10, 7267–7283,

21   doi:10.5194/acp-10-7267-2010, 2010.

22

23

24

25

26

27

28

29

Atmospheric
Chemistry
and Physics
Discussions

1 **Tables**

2

3 **Table 1. Site and data description**

Dataset	Period	Location	CCN		Size distribution		AOPs	
			Instrument	SS%	Instrument	size range	Instrument	inlet
SMEAR II	2016.1.1-2016.12.31	61° 51' N, 24° 17' E 179m	CCN-100	0.1%, 0.2%, 0.5% and 1.0%	custom-made DMPS	3-1000nm	TSI-3563 Nephelometer	PM1, PM10
SORPES	2016.06.01-2017.05.31	32°07' N, 118°56' E 40m	CCN-200	0.1%, 0.2%, 04%, and 0.8%	custom-made DMPS	6-800nm	Aurora-3000 Nephelometer	TSP
PGH[a]	2011.11.01-2013.03.25	29° 22' N, 79° 27'E 1936m	CCN-100	0.12%, 0.22%, 0.48% and 0.78%	NA	NA	TSI-3563 Nephelometer	PM1, PM10
PVC[b]	2012.07.16-2012.09.30	42° 2' N, 70° 3' W 43m	CCN-100	0.15%, 0.25%, 0.4% and 1.0%	SMPS TSI-3936	11-465nm*	TSI-3563 Nephelometer	PM1, PM10
MAO[c]	2014.01.29-2014.12.31	3° 13' S, 60° 36' W 50m	CCN-100	0.25%, 0.4%, 0.6% and 1.1%	SMPS TSI-3936	11-465nm*	TSI-3563 Nephelometer	PM1, PM10
ASI[d]	2016.06.01-2017.10.19	7° 58' S, 14° 21' W 341m	CCN-100	0.15%, 0.25%, 0.4%, and 0.8%	SMPS TSI-3936	11-465nm*	TSI-3563 Nephelometer	PM1, PM10

[a] products used: aipavg1ogrenM1.c1., and aosccnavgM1.c2.

[b] products used: aipavg1ogrenM1.s1., noaaaosccn100M1.b1., and aossmpsS1.a1.

[c] products used: aip1ogrenM1.c1., aosccn1colM1.b1., and aossmpsS1.a1.

[d] products used: aosnephdryM1.b1., aosccn2colaavgM1.b1., and aossmpsM1.a1.

4 * may vary slightly

5

6

7

8

9

Atmospheric
Chemistry
and Physics
Discussions

Open Access

1   Table 2. The slopes and offsets of the linear regressions of $R_{CCN/\sigma}$ vs. BSF at the different

2   supersaturation SS% at the studied sites. s.e.: standard error of the respective coefficient

3   obtained from the linear regressions.

SITE	SS%	$R_{CCN/\sigma} = aBSF + b$	
		$a \pm s.e.$	$b \pm s.e.$
SMEAR II	0.10%	91 ± 3	-2.9 ± 0.4
	0.20%	433 ± 5	-39 ± 0.7
	0.50%	867 ± 10	-86 ± 1.5
	1.00%	1155 ± 17	-116 ± 2.5
SORPES	0.10%	62 ± 2	-2.6 ± 0.2
	0.20%	266 ± 4	-18 ± 0.4
	0.40%	531 ± 7	-39 ± 0.8
	0.80%	738 ± 11	-56 ± 1.2
PGH	0.12%	-18 ± 1	2.6 ± 0.1
	0.22%	24 ± 3	2.8 ± 0.2
	0.48%	244 ± 12	-4.4 ± 0.8
	0.78%	344 ± 14	-8.3 ± 1.0
PVC	0.15%	417 ± 9	-30 ± 1.1
	0.25%	793 ± 17	-62 ± 2.1
	0.40%	1176 ± 25	-95 ± 3.1
	1.00%	1945 ± 43	-161 ± 5.3
MAO	0.25%	273 ± 5	-19 ± 0.7
	0.40%	544 ± 8	-43 ± 1.2
	0.60%	678 ± 13	-51 ± 1.8
	1.10%	868 ± 32	-58 ± 4.3
ASI	0.15%	22 ± 2	2.2 ± 0.2
	0.25%	105 ± 3	-3.6 ± 0.5
	0.40%	127 ± 4	-5.0 ± 0.6
	0.80%	136 ± 4	-4.0 ± 0.6

4
5

Atmospheric
Chemistry
and Physics
Discussions

1   Table 3. The coefficients a_0, a_1, b_0 and b_1 obtained from the fitting of $a = a_1\ln(SS\%) + a_0$ and b

2    $= b_1\ln(SS\%) + b_0$ with the data in Table 2. The unit of the coefficients is $[N_{CCN}]/[\sigma_{sp}] = cm^{-3}/Mm^{-1}$.

3   s.e.: standard error of the respective coefficient obtained from the regressions.

	$R_{CCN/\sigma} = (a_1 ln(SS\%) + a_0)BSF + b_1 ln(SS\%) + b_0$				SAE_{10}	
	$a_1 \pm s.e.$	$a_0 \pm s.e.$	$b_1 \pm s.e.$	$b_0 \pm s.e.$	average ± std	median
SMEAR II	464 ± 11	1170 ± 16	-49 ± 1.5	-118 ± 2.1	2.11 ± 0.67	2.22
SORPES	331 ± 12	817 ± 18	-26 ± 0.9	-62 ± 1.4	1.45 ± 0.33	1.50
PGH	205 ± 30	385 ± 41	-6.3 ± 1.5	-9.1 ± 2.0	0.53 ± 0.30	0.57
PVC	810 ± 17	1933 ± 21	-70 ± 1.7	-160 ± 2.1	1.79 ± 0.52	1.91
MAO	393 ± 45	858 ± 40	-25 ± 6.6	-60 ± 5.8	1.00 ± 0.55	1.09
ASI	64 ± 25	168 ± 31	-3 ± 2.2	-6 ± 2.7	0.73 ± 0.41	0.64

4

5

6

7

8

Atmospheric
Chemistry
and Physics
Discussions
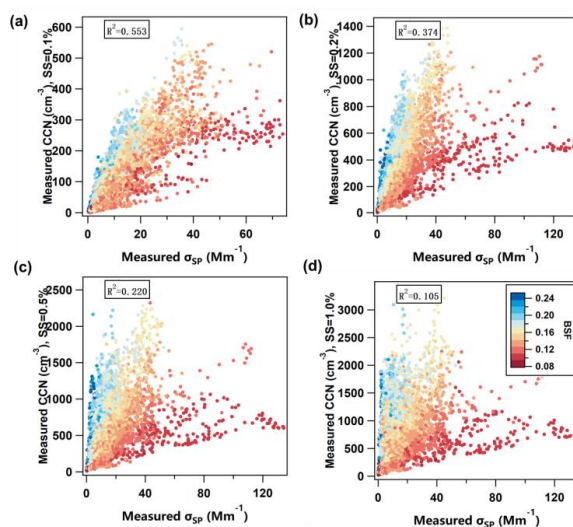
1   **FIGURES**

3   Figure 1. Measured CCN number concentration N_{CCN}(meas) vs. PM_{10} scattering coefficient σ_{sp}

4   at λ = 550 nm at SMEAR II at four supersaturations (SS%): a) 0.1 %, b) 0.2 %, c) 0.5 % and d)

5   1.0 %. Colorcoding: backscattering fraction(BSF) at λ = 550 nm.

6
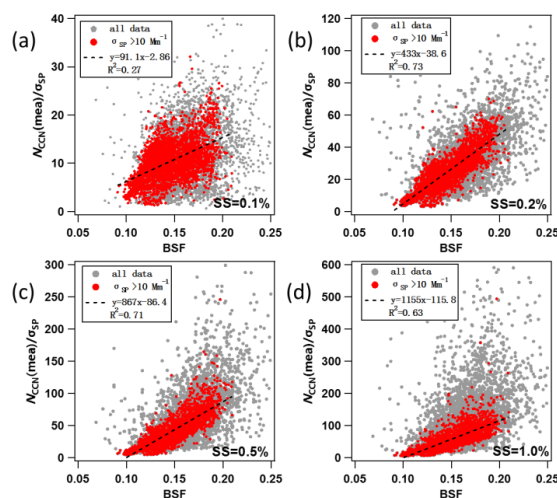
8   Figure 2. Relationship between $R_{CCN/\sigma}$ (= N_{CCN}(meas)/σ_{sp}) and BSF at SMEAR II at four

9   supersaturations (SS%): a) 0.1 %, b) 0.2 %, c) 0.5 % and d) 1.0 %. Grey symbols: all data, red

10   symbols: data at σ_{sp} > 10 Mm^{-1}. Both σ_{sp} and BSF were measured at λ = 550 nm.

Atmospheric
Chemistry
and Physics
Discussions
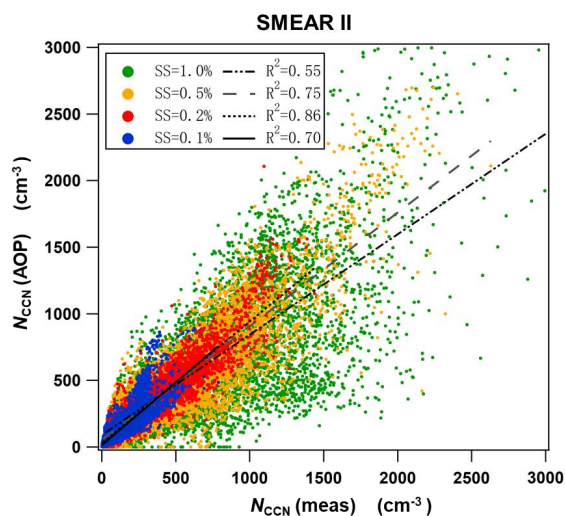
1

2   Figure 3. Comparison between $N_{CCN}(AOP_1)$ and $N_{CCN}(meas)$ at SMEAR II. $N_{CCN}(AOP)$ was

3   calculated by using the constants a and b in Table 2 for each supersaturation.
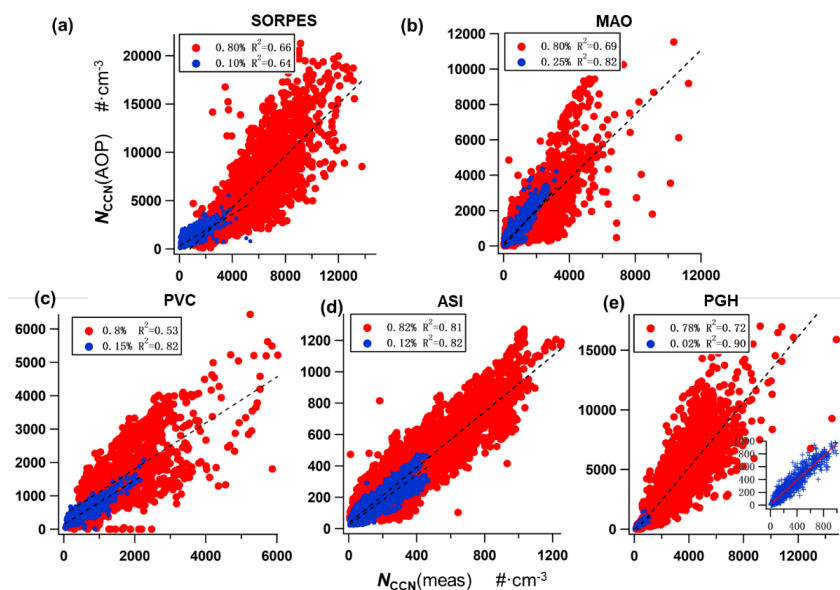
4

5   Figure 4. $N_{CCN}(AOP_1)$ vs. $N_{CCN}(meas)$ at a) SORPES, b) MAO, c) PVC, d) ASI and e) PGH. $N_{CCN}(AOP)$

6   was calculated by using the constants a and b in Table 2 for each supersaturation.

7
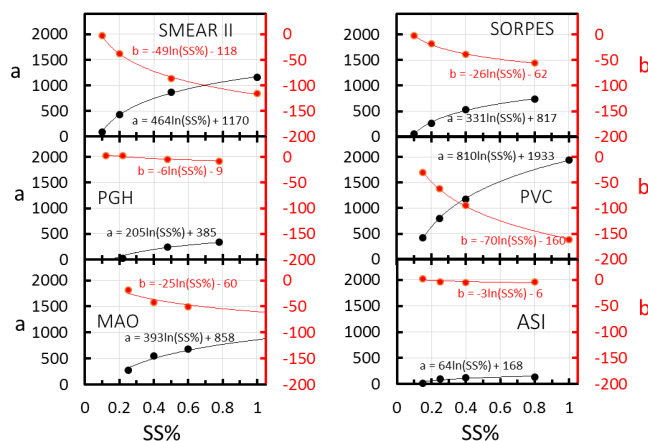
1

2   Figure 5. The coefficients a and b of each station (Table 2) as a function of supersaturation.

3
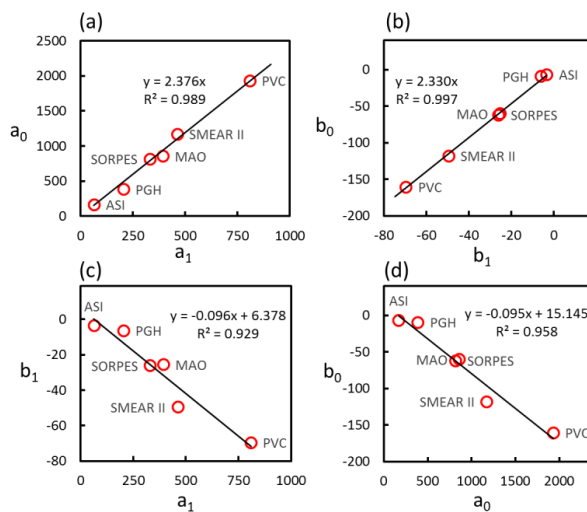
4

5   Figure 6. Relationship between the coefficients of Equation (5) presented in Table 2 for the 6

6   stations. a) a_0 vs. a_1, b) b_0 vs. b_1, c) b_1 vs. a_1, d) b_0 vs. a_0.

7

8

9

10
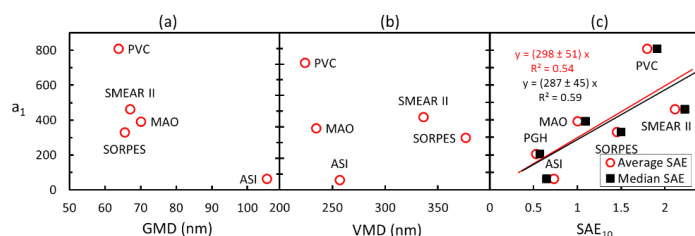
1

2   Figure 7. Relationship of the a_1 coefficient in Equation (6) with the average a) geometric mean

3   diameter of the PNSD data size ranges of the sites, b) volume mean diameter of the same size

4   range, and c) PM_{10} scattering Ångström exponent (SAE10).

5
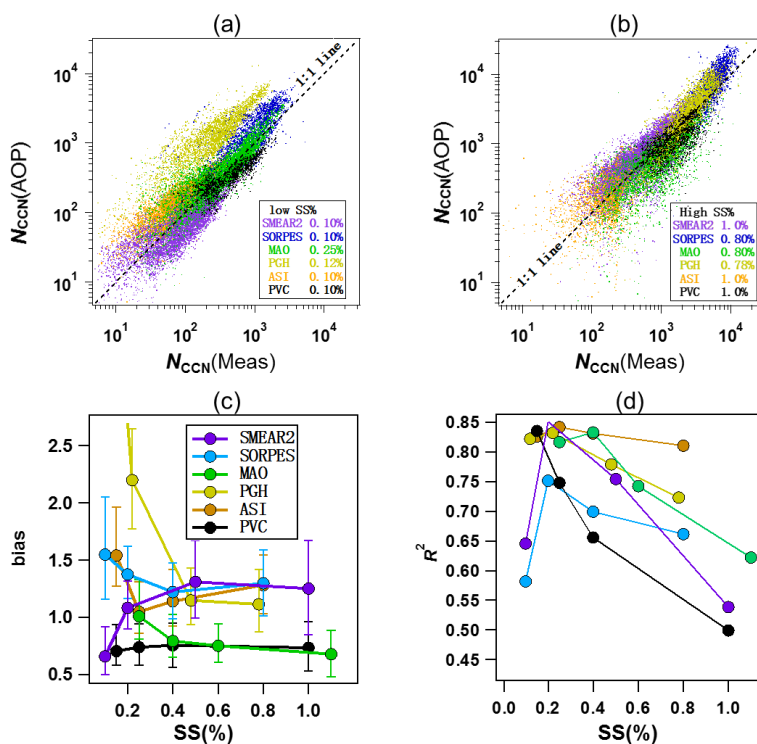
6

7   Figure 8. Statistics of $N_{CCN}(AOP_2)$ from parameterization 2. $N_{CCN}(AOP_2)$ vs. N_{CCN}(meas) at

8   different sites at relatively (a) low and (b) high supersaturations, (c) bias = $N_{CCN}(AOP_2)$/ N_{CCN}

9   (meas) at different sites and supersaturations, and (d) R^2 of the linear regression of $N_{CCN}(AOP_2)$

10   vs. N_{CCN} (meas) at different sites and supersaturations.

11
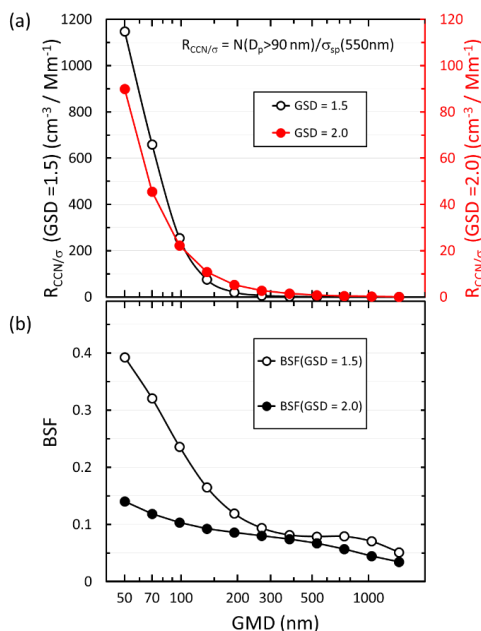
1

2   Figure 9. Size distribution of a) $R_{CCN/\sigma}$ and b) backscatter fraction BSF (λ = 550 nm) of simulated

3   narrow (GSD = 1.5) and wide (GSD = 2.0) unimodal size distributions. GMD: geometric mean

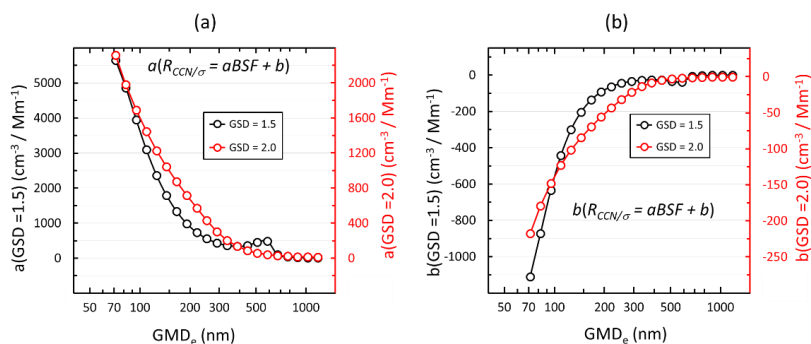4   diameter, GSD: geometric standard deviation.
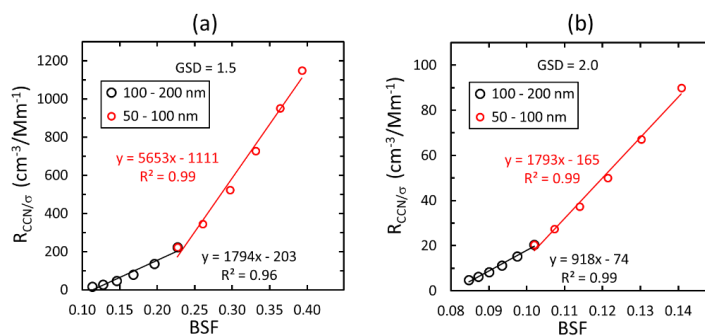
5

6   Figure 10. Linear regressions of $R_{CCN/\sigma}$ vs backscatter fraction BSF (λ = 550 nm) of simulated

7   unimodal a) narrow (GSD = 1.5) and b) wide (GSD = 2.0) size distributions. The regressions

8   were calculated assuming that the data consist of size distributions with GMD ranging from 50

9   to 100 nm and 100 to 200 nm.

10

1

2 Figure 11. Size distributions of the coefficients of the linear regressions of $R_{CCN/\sigma}(\lambda = 550$ nm)

3 vs backscatter fraction BSF ($\lambda = 550$ nm) of narrow and wide size distributions. a) slopes of

4 $R_{CCN/\sigma}$ vs. BSF, b) offsets of $R_{CCN/\sigma}$ vs. BSF. $R_{CCN/\sigma}$ was calculated assuming particles larger than

5 90 nm get activated. The regressions were calculated for 5 consecutive size distributions.

6 GMD_e is the geometric mean of the range of the unimodal size distributions used for the

7 regressions.

8

1

2
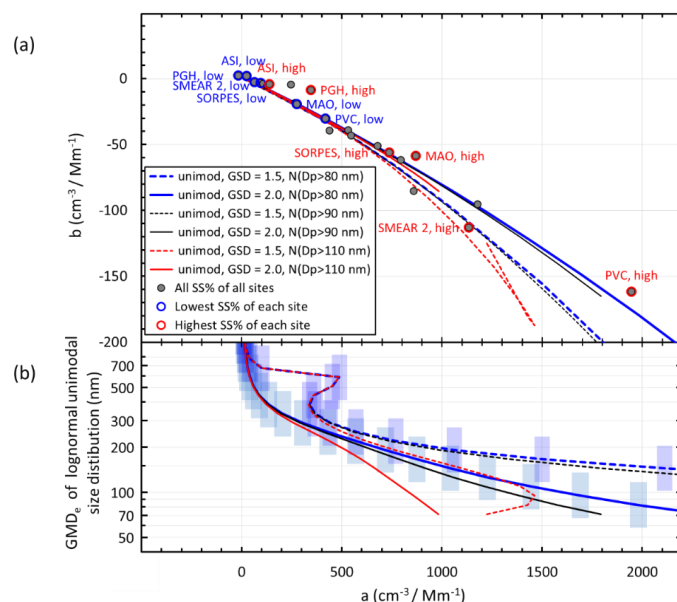
Figure 12. a) Relationships of the slopes and offsets of the linear regressions $R_{CCN/\sigma}$ = aBSF + b

of the simulated unimodal narrow (GSD = 1.5) and wide (GSD = 2.0) size distributions and those

obtained from the similar regressions of the station data at low and high supersaturations

(Table 2). b) Equivalent geometric mean diameter (GMD_e) of the unimodal modes used for the

linear regression vs. the slope of the linear regression of $R_{CCN/\sigma}$ vs. BSF. The vertical error bars

show the ranges of the GMDs of the unimodal size distributions used in the respective linear
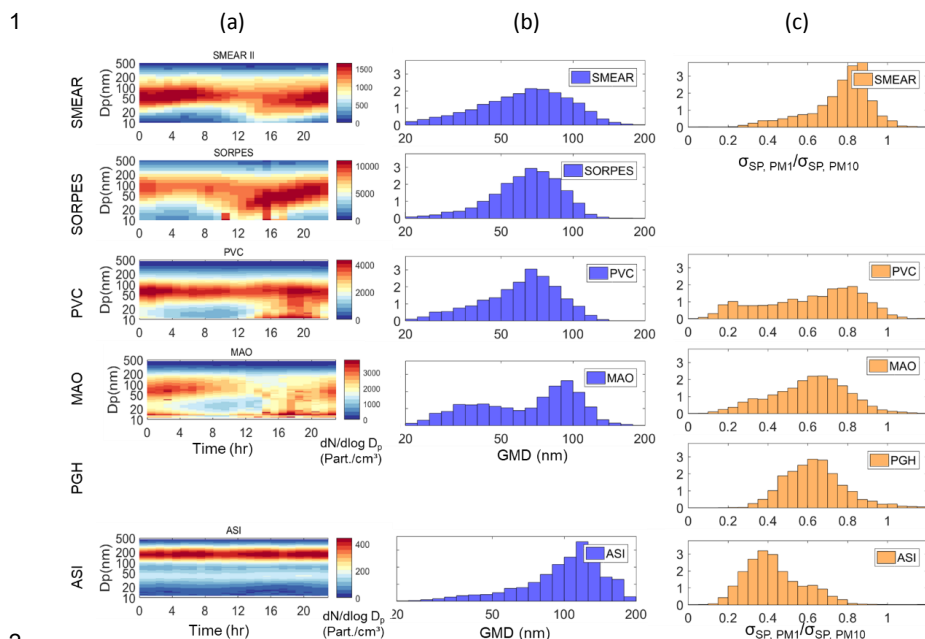
regressions.

1

2

3 Figure 13. Analyses of particle size distributions at the six sites. a) Average diurnal cycle of

4 PNSD and b) normalized size distribution of GMD at SMEAR II, SORPES, PVC, and ASI, c)

5 normalized frequency distribution of $\sigma_{sp}(PM_1)/\sigma_{sp}(PM_{10})$ at SMEAR II, PVC, MAO, PGH and ASI.

6